Study of aluminium oxide thin films deposited by plasma-enhanced atomic layer deposition from tri-methyl-aluminium and dioxygen precursors: investigation of interfacial and structural properties

Ahmet Lale, Emmanuel Scheid, Fuccio Cristiano, Lucien Datas, Benjamin Reig, Jérôme Launay, Pierre Temple-Boyer

Study of aluminium oxide thin films deposited by plasma-enhanced atomic layer deposition

from tri-methyl-aluminium and dioxygen precursors:

investigation of interfacial and structural properties

A. Lale[1,2], E. Scheid[1,2], F. Cristiano[1,2], L. Datas[3], B. Reig[1,2], J. Launay[1,2], Pierre Temple-Boyer[1,2]

[1] CNRS, LAAS, 7 avenue du colonel Roche, F-31400 Toulouse, France

[2] Université de Toulouse, UPS, LAAS, F-31400 Toulouse, France

[3] Université de Toulouse, Centre de microcaractérisation Raimond Castaing, F-31400 Toulouse, France

Abstract:

Aluminium oxide (Al_2O_3) films were deposited on silicon substrates using plasma-enhanced atomic layer deposition (PE-ALD) technique with tri-methyl-aluminium TMA ($Al(CH_3)_3$) and dioxygen (O_2) as precursors. PE-ALD experiments were performed in order to (i) investigate the interfacial properties between the silicon substrate and the alumina layer, and (ii) understand the impact of growth and crystallization phenomena on the Al_2O_3 films properties (structural, optical, mechanical, dielectric and etch). The formation of oxide-based transition layers, either silicon oxide SiO_2 and/or aluminosilicate Al_xSi_yO, was evidenced for the TMA/O_2 PE-ALD process. Based on these results, it appears that no substrate-enhanced growth occurs at the early stages of the growth process, as assumed in previous reports. Thus, constant growth rate (0.08 nm per cycle) and refractive index (1.64 at a 450 nm wavelength) were obtained for the Al_2O_3 layer deposited at 300°C. Finally, thermal annealing experiments were performed on these films, evidencing the influences of atomic structural rearrangement and crystallization on the Al_2O_3 film main characteristics: interface steepness, atomic structure, refractive index, residual stress, dielectric constant and etch rate.
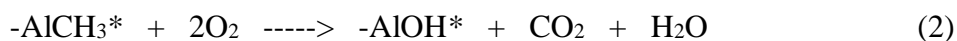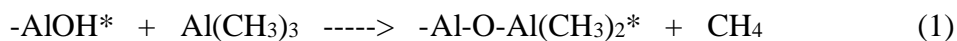
1. Introduction

In the frame of microtechnologies, aluminium oxide (Al_2O_3) has been investigated for several applications: as a "high-k" material for MOS gate oxide [1,2], as an ion-sensitive and passivation layer for FET-based microsensors [3,4], as a passivation layer for OLED and solar cell devices [5,6], as a luminescent material for dosimeters [7],... As a consequence, many processes based on physical and/or chemical deposition techniques were developed in order to integrate alumina thin films with optimized properties into the corresponding fabrication processes: electron beam evaporation [8,9], pulsed laser deposition [10], sputtering [11], chemical vapour deposition [12], metal-organic chemical vapour deposition [13], plasma-enhanced chemical vapour deposition [14],... Among them, atomic layer deposition (ALD) was thoroughly studied for the conformal deposition of Al_2O_3 thin films [15-17], emphasizing the use of tri-methyl-aluminium $Al(CH_3)_3$ (also called TMA) as an aluminium source and water (H_2O) as an oxidant source [18-25]. Nevertheless, other sources such aluminium trichloride ($AlCl_3$) as well as dioxygen (O_2) and ozone (O_3), were also developed in parallel using plasma-enhanced atomic layer deposition (PE-ALD) in order to reduce the impurity content in the grown Al_2O_3 film and improve their dielectric properties [24-28].

In the different studies related to the ALD process [18-28], the presence of a steep interface was systematically assumed between the Al_2O_3 films and the silicon substrate, which allows simplifying the determination of the ALD growth rate per cycle as well as defining different growth types: linear, substrate-enhanced and substrate-inhibited [29]. This "steep interface" assumption seems obvious when considering the atomic layer deposition principles. Nevertheless, since other physical and chemical phenomena occur during the ALD process, it seems crucial to investigate the ALD film layer structure in more detail [30]. This paper proposes, firstly, to investigate the interfacial properties between the silicon substrate and PE-ALD alumina thin films deposited from

Al(CH$_3$)$_3$/O$_2$ precursors, and, secondly, to study the structural, optical, mechanical and dielectric properties of the grown layers, focusing on the impact of a post-growth rapid thermal anneal step (in the 500°C – 1100°C temperature range) on their evolution.

2. Experimental details

Growth experiments were carried out in a FIJI F200 ALD equipment developed by CAMBRIDGE NANOTECH company. Prior to deposition, 100mm (100) silicon substrates were cleaned into diluted hydrofluoric acid (HF – 10%) to remove any oxide layer. After this HF cleaning, the native SiO$_2$ layer was still estimated around 0.7 nm by ellipsometry. Then, Al$_2$O$_3$ films were deposited using conventional experimental conditions (deposition temperature: 300°C, base pressure: ~ 70 mTorr) from tri-methyl-aluminium Al(CH$_3$)$_3$ (TMA) and dioxygen (O$_2$) according to a standard routine: TMA injection in gaseous phase (injection duration: 0.025 s), purge (argon: 180 sccm, duration: 6 s), plasma O$_2$ exposure (O$_2$: 20 sccm, plasma power: 300 W), purge (argon: 180 sccm, duration: 6 s). These experimental conditions and durations were chosen in order to saturate the ALD growth rate while preventing any undesirable gaseous mixing [24,25,27]. Thus, Al$_2$O$_3$ growth occurs according to the binary reaction sequence [31]:

$$-AlOH^* \ + \ Al(CH_3)_3 \ -----> \ -Al-O-Al(CH_3)_2^* \ + \ CH_4 \qquad (1)$$
$$-AlCH_3^* \ + \ 2O_2 \ -----> \ -AlOH^* \ + \ CO_2 \ + \ H_2O \qquad (2)$$

where -AlOH*, -Al-O-Al(CH$_3$)$_2$* and -AlCH$_3$* represent surface species while monofunctional adsorption is assumed for simplification.

Thermal anneals were performed in an AnnealSys AS-Master-2000HT rapid thermal process (RTP) equipment using two different gaseous atmospheres (N$_2$/H$_2$ or O$_2$). Aluminium oxide films

were etched using (i) phosphoric and hydrofluoric acids (H_3PO_4 85% and HF 5%) for wet etching as well as (ii) a Cl_2 dry etching gas in an ICP-RIE (Inductively coupled plasma reactive ion etching) Trikon Omega 201 equipment (ICP power: 500 W, bias power: 25–100 W) [32].

Structural, optical, mechanical and dielectric properties of aluminium oxide thin films were studied using numerous characterisation techniques. Alumina films were studied by spectroscopic ellipsometry using an Uvisel equipment from Horiba Jobin Yvon, in order to estimate deposited thicknesses as well as optical indexes at a 450 nm wavelength. Growth rates per ALD cycle were finally calculated by dividing the deposited thickness by the ALD cycle number. The accuracy of these measurements was estimated to be ± 2%.

Wafer curvature measurements before and after PE-ALD film deposition were also performed by profilometry. Since the deposited films were very thin compared to the silicon substrate (thickness: ~ 500 µm), their residual stress was finally calculated thanks to the Stoney's formula [33,34]. The accuracy of the whole technique was estimated at ± 5%.

Dielectric properties were studied using a mercury probe (MDC company, model 802C) coupled with an Agilent 4294A impedance analyser. Using a 4.18×10^{-3} cm^2 mercury contact area, C-V experiments were performed between -10 V and +10 V for a 100 mV sinusoidal signal at 1, 10, 100 and 1000 kHz. Thus, alumina dielectric constant was calculated from the capacitance value in accumulation thanks to the standard planar capacitor equation. The accuracy of the whole technique was estimated at ± 5%.

TEM (Transmission electron microscopy) was performed in a TEM JEOL JEM-ARM200F cold FEG, STEM corrected, equipment installed in the French "Centre de microcaractérisation Raimond Castaing" (Toulouse, France). At 200 kV, its point-to-point resolution is 0.19 nm in TEM mode (0.078 nm in STEM mode). It is coupled with an EDX (Energy Dispersive X-ray) spectrometer JEOL CENTURIO in order to analyse atomic compositions at the nanoscale (resolution: 2 nm). Before the experiments, the EDX spectrometer was calibrated using a

monocrystalline sapphire sample. Then, ~100 nm-thin TEM samples were prepared from Al_2O_3 films using a FEI Helios 600i FIB (Focused Ion Beam) equipment. GIXRD (Grazing Incidence X-ray Diffraction) experiments were also performed using a Bruker D8 Discovery diffractometer (X-ray source and associated wavelength: $K\alpha 1$ copper, 0.154056 nm) in order to study alumina film crystallinity.

3. Results and discussion

3.1. Mean growth rate per ALD cycle and refractive index

Alumina films characteristics were studied by spectroscopic ellipsometry taking into account the 0.7 nm native silicon oxide layer present after HF clean. Thus, assuming steep interfaces for the $Si/SiO_2/Al_2O_3$ structure, the deposited thickness, i.e. the mean growth rate per ALD cycle g_r, as well as the refractive index at a 450 nm wavelength n_{450nm} were estimated (figure 1). From these first results, the studied TMA/O_2 PE-ALD process appears to be characterized by a substrate-enhanced growth [29] with an apparent g_r value around 0.09 ± 0.01 nm for the highest number of ALD cycles. Nevertheless, the associated refractive index variations are quite surprising since the n_{450nm} apparent value increases from 1.47 (i.e. similar to silicon dioxide SiO_2) at the early stages of the growth, up to 1.67 for the highest number of cycles, i.e. far lower than the value known for bulk monocrystalline alumina or sapphire: $n_{450nm} = 1.78$ [35].

In order to check the steepness of the different interfaces and to have a better analysis of these results, TMA/O_2 samples were characterized by TEM coupled with EDX spectrometry. For the thinnest samples (number of cycles: 30 and 60), investigations evidenced a thickness increase of the initial native oxide layer (0.7 nm), accompanied by the formation of an Al_xSi_yO aluminosilicate overlayer (figures 2a and 2b). On the contrary, for the thickest samples (number of cycles: 300 and 600) no SiO_2 layer is observed. Instead, an Al_xSi_yO/Al_2O_3 structure is formed (figures 3a and 3b).

5

The different transition layers (cf. dashed lines in figures 2b and 3b) are determined from the variation of the atomic profiles extracted from the intensity of the different EDX peaks (arbitrary units). In the case of the upper alumina layer in samples with a high number of cycles, it was possible to quantify the EDX spectra and confirm the effective deposition of a stoichiometric Al_2O_3 alumina layer. The mean values of the different layer thicknesses are given in table 1.

According to these results, it appears that, for ALD cycle number lower than 100 (i.e. for film thickness lower than 10 nm), silicon oxidation occurs during the "TMA injection - plasma O_2" routine. Since only native oxide is present on the silicon substrate, this phenomenon is responsible for the growth of the underlayer oxide layer. Moreover, rather than an alumina Al_2O_3 film, an aluminosilicate Al_xSi_yO one is simultaneously formed on top, leading to the formation of a SiO_2/Al_xSi_yO structure. On the contrary, for ALD cycle number higher than 200 (i.e. for film thickness higher than 20 nm), the TMA/O_2 PE-ALD routine is efficient and allows to effectively deposit alumina atomic layers on top, leading to a final Al_xSi_yO/Al_2O_3 structure.

Such experiments clearly show that silicon oxidation and the associated diffusion phenomena interfere with the TMA/O_2 PE-ALD process. This scenario was confirmed by studying a 300-cycle PE-ALD films deposited on top of a thermally oxidized silicon substrate (SiO_2 thickness: ~10 nm, cf. table 1, bottom row). In this case, considering the TEM/EDX resolution (2 nm), no aluminosilicate layer was evidenced and only alumina was effectively deposited, leading to a final SiO_2/Al_2O_3 structure with steep interfaces (figure 4). Such result is consistent with the interference of silicon oxidation during the first ALD cycles: the thicker the oxide underlayer, the less effective the silicon oxidation phenomenon will be, resulting in a thinner aluminosilicate intermediate layer.

As a matter of fact, it finally appears that the initial SiO_2/Al_xSi_yO bilayer transforms into an aluminosilicate monolayer prior to forming the final Al_xSi_yO/Al_2O_3 structure. Such transition is expected to be controlled by the diffusion of oxygen, aluminium and silicon atoms during the PE-ALD process (performed at 300°C), as already shown for hafnium oxide thin films deposited by

ALD [36]. In order to check this assumption, the 600-cycle Al_xSi_yO/Al_2O_3 film was annealed for 5 minutes under an O_2 gaseous atmosphere at different temperatures (750°C and 900°C). Indeed, TEM/EDX characterizations showed that the aluminosilicate Al_xSi_yO underlayer broke up in order to participate to the formation of both SiO_2 lower layer and Al_2O_3 upper layer (table 2 and figure 5). Thus, the thermal diffusion and rearrangement of oxygen, aluminium and silicon atoms into a $Si/SiO_2/Al_2O_3$ structure with steep interfaces was effectively demonstrated.

In view of these results, the values of film deposited thickness and refractive index, initially determined by spectroscopic ellipsometry, were reconsidered assuming the formation of a $SiO_2/Al_xSi_yO/Al_2O_3$ structure in all samples, independently of the number of PE-ALD cycles. Thus, in all cases, the refractive index at a 450 nm wavelength n_{450nm} of the Al_2O_3 upper layer was estimated around 1.64. In parallel, the mean growth rate per ALD cycle g_r was finally estimated around 0.08 ± 0.005 nm whatever the number of ALD cycles.

Thus, it is finally shown that the TMA/O_2 PE-ALD process is not characterized by steep interfaces. For low ALD cycle numbers (lower than 100), the "TMA injection – plasma O_2" routine is responsible for the silicon substrate oxidation, i.e. for the growth of a SiO_2 underlayer, and, subsequently, for the deposition of an Al_xSi_yO aluminosilicate film. Taking into account this phenomenon, it is clear that no substrate-enhanced growth occurs at the early stages of the growth process, as previously assumed. Indeed, apart for the initial regime, the TMA/O_2 PE-ALD process occurs in a standard way, allowing the deposition of stoichiometric alumina Al_2O_3 with a linear growth mechanism, i.e. with a constant growth rate.

In the following, investigations will focus on the physical/chemical properties of TMA/O_2 PE-ALD films obtained for high numbers of ALD cycles (higher than 400). For such high ALD cycle numbers, the influence of the aluminosilicate Al_xSi_yO lower layer is negligible (figure 1), allowing to consider a global SiO_2/Al_2O_3 structure. According to our analyses, this assumption is related to

7

measurement errors around ± 4% for the alumina film thickness and related parameters (see hereafter).

3.2. Thermal annealing influences

Since as-deposited alumina films were characterized by refractive index lower than expected, the influence of thermal annealing was investigated in detail. Thus, different rapid thermal annealing processes (duration: 5 minutes, gaseous atmospheres: N_2/H_2 and O_2) were performed at increasing temperatures, i.e. from 500 to 1100°C, on different 400-cycle alumina samples. In both gaseous ambiences, the refractive index at a 450nm wavelength was found to increase with annealing temperature (figure 6). Starting at 750°C from the as-deposited n_{450nm} value around 1.64, a sigmoidal variation was evidenced to reach a final n_{450nm} value around 1.72. Since such variations were already evidenced for ALD alumina films [37] and associated to crystallization phenomena for CVD silicon film [34], X-ray diffraction analysis was performed on the different samples. According to a previous study [38], XRD spectra were studied in the [30° - 72°] 2θ angle range and more precisely around 67.8° (figures 7a and 7b). At this 2θ angle value, starting at 800°C, the temperature increase is responsible for the appearance of an intensity peak that was previously related to crystallization phenomena (figures 7b and 7c). Thus, the refractive index n_{450nm} increase with annealing temperature was effectively related to the transition from amorphous to polycrystalline alumina. As a result, the corresponding values were determined:

- PE-ALD amorphous alumina: $n_{450nm} \approx 1.64$ (1)

- PE-ALD polycrystalline alumina: $n_{450nm} \approx 1.72$ (2)

The n_{450nm} value obtained for polycrystalline alumina was still lower than 1.78, evidenced for bulk monocrystalline alumina or sapphire [35]. As already shown for monocrystalline and

polycrystalline silicon [34], this discrepancy might be associated to the presence of amorphous grain boundaries in the polycrystalline Al_2O_3 films (figure 8).

3.3. Residual stress

The residual stress σ of the different 900-cycle TMA/O_2 PE-ALD films was studied by wafer curvature measurements and calculated using the Stoney equation while considering a SiO_2/Al_2O_3 bilayer. Independently of the gaseous atmosphere (N_2/H_2 and O_2), similar variations were evidenced as a function of the annealing temperature (figure 9).

Initially, the as-deposited alumina films were characterized by a "no-stress" configuration ($\sigma \approx +10$ MPa). Then, a first increase was evidenced between 500 and 700°C to reach a +300 MPa tensile stress. This phenomenon could be related to the diffusion of oxygen, aluminium and silicon atoms into the film occurring at such temperature and therefore associated to the rearrangement of the Al_xSi_yO/Al_2O_3 structure towards the SiO_2/Al_2O_3 one (see section 3.1 above). Then, a second sharp increase was evidenced between 750 and 800°C to reach very high tensile stress values ($\sigma \approx +2200$ MPa). As shown by Krautheim et al. [39] and as seen previously (see section 3.2 above), this phenomenon should be related to film crystallization and therefore to the transition from amorphous to polycrystalline alumina. However, if a sigmoidal stress variation was expected (as shown for amorphous silicon crystallization [34]), a third phenomenon responsible for compressive stress was shown to interfere for temperature higher than 800°C. Thus, a stress decrease was finally evidenced for the highest temperatures. This last phenomenon is not clearly explained. Since it was obtained for both gaseous atmosphere (N_2/H_2 and O_2), it cannot be due to silicon oxidation phenomena (negligible for stress measurement) but should be related to some phase transition into polycrystalline alumina [39].

3.4. Dielectric constant

The dielectric constant ε_r of different 400-cycle TMA/O_2 PE-ALD films was studied by capacitance-voltage (C-V) measurements at different frequencies (1, 10, 100 and 1000 kHz) and analysed as a function of the annealing temperature (gaseous atmosphere: O_2). Measured C-V curves are characteristics of a Metal-Insulator-Silicon capacitive structure (results not shown), enabling the determination of the capacitance in accumulation C_{acc}. Finally, the insulator equivalent dielectric constant ε_r was estimated using the planar capacitor equation while considering a SiO_2/Al_2O_3 bilayer. As shown for the refractive index n_{450nm} (see section 3.2 above), a typical sigmoidal variation was obtained, evidencing a dielectric constant increase from 8.5 to 10.2 with temperature (figure 10). Again, this variation should be related to crystallization phenomena of alumina between 750 and 850°C. As a result, the dielectric constants of amorphous and polycrystalline alumina were determined:

$$- \text{PE-ALD amorphous alumina: } \varepsilon_r \approx 8.5 \qquad (3)$$

$$- \text{PE-ALD polycrystalline alumina: } \varepsilon_r \approx 10.2 \qquad (4)$$

These ε values are in good agreement with standard value obtained for bulk monocrystalline alumina or sapphire [40].

3.5. Etch properties

Since the integration of TMA/O_2-based Al_2O_3 PE-ALD films is planned for the realization of microtechnological devices, their chemical and physical etch properties were also studied (table 3). Concerning wet etching, phosphoric acid H_3PO_4 was found to be ineffective while hydrofluoric acid HF was only effective for amorphous Al_2O_3 (etch rate: 40 nm/min). In order to etch polycrystalline Al_2O_3, a Cl_2-based dry etch in an ICP-RIE equipment was implemented. Thus, depending on the ICP power, the etch rate was found to increase linearly up to 90 nm/min for amorphous Al_2O_3,

while it saturates at a maximal value of 40 nm/min for polycrystalline Al_2O_3. According to our results, a bias power of 50 W is proposed in order to effectively and selectively etch any TMA/O_2-based Al_2O_3 PE-ALD films.

4. Conclusion

In summary, PE-ALD Al_2O_3 thin films (thickness range: $6 - 72$ nm) were deposited on silicon substrates using TMA/O_2 precursors. TEM/EDX investigations evidenced the formation of different transition layers depending on the number of ALD cycles. For low ALD cycle numbers (lower than 100), it was demonstrated that the TMA/O_2 PE-ALD routine is not efficient to deposit alumina atomic layers because of silicon oxidation phenomena. As a result, the initial formation of a SiO_2/Al_xSi_yO transition structure with no steep interface was shown. For high ALD cycle numbers (higher than 200), oxidation phenomena are inhibited due to the higher deposited thickness so that the TMA/O_2 PE-ALD process operates normally to form alumina layers. Nevertheless, diffusion and rearrangement of oxygen, aluminium and silicon atoms were found to interfere with the PE-ALD process, leading to the formation of an aluminosilicate Al_xSi_yO transition layer and the deposition of a final Al_xSi_yO/Al_2O_3 stack. In view of these different mechanisms, no "substrate-enhanced growth" phenomenon was finally evidenced for the TMA/O_2 PE-ALD process. As a result, a constant growth rate (0.08 nm per cycle) and refractive index (1.64 at a 450 nm wavelength) were obtained for the deposited Al_2O_3 upper layer, independently of the number of ALD cycles.

The influence of post-growth thermal annealing was also investigated. Thanks to XRD analysis, crystallization of Al_2O_3 films was found to start at a temperature of 750°C. Then, thermally induced atomic rearrangement within the Al_2O_3 structure was found to be responsible for sigmoidal increases of various parameters with increasing temperature, such as the refractive index

at a 450 nm wavelength n_{450nm}, the residual stress σ and the dielectric constant ε_r. Thus, the corresponding properties of amorphous and polycrystalline alumina were finally determined. The results obtained in this work allow to have a better understanding of the PE-ALD-Al_2O_3 film deposition process and related properties. They will be helpful for the integration of thick (> 20 nm) alumina layers in the frame of micro/nano-technological applications.

References

[1] R.M. Wallace and G.D. Wilk, "High-k dielectric materials for microelectronics", Critical Reviews in Solid State and Materials Sciences, 28 (2003) 231-285

[2] J.A. Kittl, K. Opsomer, M. Popovici, N. Menou, B. Kaczer, X.P. Wang, C. Adelmann, M.A. Pawlak, K. Tomida, A. Rothschild, B. Govoreanu, R. Degraeve, M. Schaekers, M. Zahid, A. Delabie, J. Meersschaut, W. Polspoel, S. Clima, G. Pourtois, W. Knaepen, C. Detavernier, V.V. Afanas'ev, T. Blomberg, D. Pierreux, J. Swerts, P. Fischer, J.W. Maes, D. Manger, W. Vandervorst, T. Conard, A. Franquet, P. Favia, H. Bender, B. Brijs, S. Van Elshocht, M. Jurczak, J. Van Houdt, D.J. Wouters, "high-k dielectrics for future generation memory devices", Microelectronic Engineering, 86 (2009) 1789-1795

[3] O. Knopfmacher, A. Tarasov, W. Fu, M. Wypf, B. Niesen, M. Calame and C. Schönenberger, "Nernst limit in dual-gated Si-nanowire FET sensors", Nanoletters, 10 (2010) 040802 1-

[4] S. Chen, J.G. Bomer, E.T. Carlen and A. van den Berg, "Al_2O_3/silicon nanoISFET with near ideal Nernstian response", Nanoletters, 11 (2011) 2334-2341

[5]   G. Dingemans and E. Kessels, "Status and prospects of Al_2O_3-based surface passivation for silicon solar cells", Journal of Vacuum Science and Technology, A30 (2012) 040802

[6]   T. Maindron, B. Aventurier, A. Ghazouani, T. Jullien, N. Rochat, J.Y. Simon and E. Viasnoff, "Investigation of Al_2O_3 barrier film properties made by atomic layer deposition onto fluorescent tris-(8-hydroxyquinoline) aluminium molecular films", Thin Solid Films, 548 (2013) 517-525

[7]   E.G. Yukihara and S.W.S. Mac Heever, "Optically stimulated luminescence dosimetry in medicine", Physics in Medicine and Biology, 53 (2008) R351-R379

[8]   J. Proost and F. Spaegen, "Evolution of the growth stress stiffness and microstructure of alumina thin films during vapour deposition", Journal of Applied Physics, 91 (2004) 204-216

[9]   P. Nayar, A. Khanna, D. Kabiraj, S.R. Abhilash, B.D. Beake, Y. Losset and B. Chen, "Structural, optical and mechanical properties of amorphous and crystalline alumina thin films", Thin Solid Films, 568 (2014) 19-24

[10]   C. Hibert, H. Hidalgo, C. Champeaux, P. Tristant, C. Tixier, J. Desmaison and A. Catherinot, "Properties of aluminum oxide thin films deposited by pulsed laser deposition and plasma enhanced chemical vapour deposition", Thin Solid Films, 516 (2008) 1290-1296

[11]   P.J. Kelly and R.D. Arnell, "Control of the structure and properties of aluminum oxide coating by pulsed magnetron sputtering", Journal of Vacuum Science and Technology, A17 (1999) 945-953

[12]   S. Ruppi, "Deposition, microstructure and properties of texture-controlled CVD α-Al_2O_3 coatings", International Journal of Refractory Metals and Hard Materials, 23 (2005) 306-316

[13]   Q.Y. Shao, A.D. Li, H.Q. Ling, D. Wu, Y. Wang, Y. Feng, S.Z. Yang, Z.G. Liu, M. Wang and N.B. Ming, "Growth and characterization of Al_2O_3 gate dielectric films by low-pressure metalorganic chemical vapor deposition", Microelectronic engineering, 66 (2003) 842-848

[14]   R.S. Johnson, G. Lucovski and Isreal Baumvol, "Physical and electrical properties of nanocrystalline prepared by remote plasma enhanced chemical vapour deposition", Journal of Vacuum Science and Technology, A19 (2001) 1353-1360

[15]   M. Leskelä and M. Ritala, "Atomic layer deposition (ALD): from precursors to films structures", Thin Solid Films, 409 (2002) 138-146

[16]   O. Sneh, R.B. Clark-Phelps, A.R. Londergan, J. Winkler and T.E. Seidel, "Thin film atomic layer deposition equipment for semiconductor processing", Thin Solid Films, 402 (2002) 248-261

[17]   R.L. Puurunen, "Surface chemistry of atomic layer deposition: a case study for the trimethylaluminum/water process", Journal of Applied Physics, 97 (2005) 121301

[18]   A.W. Ott, J.W. Klaus, J.M. Johnson and S.M. George, "Al_2O_3 thin film growth on Si (100) using binary sequence chemistry", Thin Solid Films, 292 (1997) 135-144

[19]   S.J. Yun, K.H. Lee, J. Skarp, H.R. Kim and K.S. Nam, "Dependence of atomic layer-deposited Al_2O_3 films characteristics on growth temperature and Al precursors of $Al(CH_3)_3$ and $AlCl_3$", Journal of Vacuum Science and Technology, A15 (1997) 2993-2997

[20]   R. Matero, A. Rahtu, M. Rittala, M. Leskelä and T. Sajavaara, "Effect of water dose on the atomic layer deposition rate of oxide thin films", Thin Solid Films, 368 (2000) 1-7

[21]   J.W. Elam, M.D. Groner and S.M. George, "Viscous flow reactor with quartz microbalance for thin film growth by atomic layer deposition", Review of Scientific Instruments, 73 (2002) 2981-2987

[22]   C. Barbos, D. Blanc-Pelissier, A. Fave, E. Blanquet, A. Crisci, E. Fourmond, D. Albertini, A. Sabac, K. Ayadi, P. Girard and M. Lemiti, "Characterization of Al_2O_3 thin films prepared by thermal ALD", Energy Procedia, 77 (2015) 558-564

[23] P. Borylo, K. Lukaszkowicz, M. Szindler, J. Kubacki, K. Balin, M. Basiaga and J. Szewczenko, "Structure and properties of Al_2O_3 thin films deposited by ALD process", Vaccum, 131 (2016) 319-326

[24] S.C. Ha, E. Choi, S.H. Kim and J.S. Roh, "Influence of oxidant source on the property of atomic layer deposited Al_2O_3 on hydrogen-terminated Si substrate", Thin Solid Films, 476 (2005) 252-257

[25] J.L. Van Hemmen, S.B.S. Heil, J.H. Klootwijk, F. Roozeboom, C.J. Hodson, M.C.M. van de Sanden and W.M.M. Kessels, "Plasma and thermal ALD of Al_2O_3 in a commercial 200 mm ALD reactor", Journal of the Electrochemical Society, 154 (2007) G165-G169

[26] V.R. Rai, V. Vandalon and S. Agarwal, "Influence of surface temperature on the mechanism of atomic layer deposition of aluminum oxide using an oxygen plasma and ozone", Langmuir, 28 (2012) 350-357

[27] S.E. Potts, H.B. Profikt, R. Roelofs and W.M.M. Kessels, "Room-temperature ALD of metal oxide thin films by energy-enhanced ALD", Chemical Vapor Deposition, 19 (2013) 125-133

[28] L. Aarik, T. Arroval, R. Rammula, H. Mändar, V. Sammelselg, B. Hudec, K. Husekova, K. Fröhlich and J. Aarik, "Atomic layer deposition of high-quality Al_2O_3 and Al-doped TiO_2 thin films from hydrogen-free precursors", Thin Solid Films, 565 (2014) 19-24

[29] R.L. Puurunen and W. Vandervorst, "Island growth as a growth model in atomic layer deposition: a phenomenological model", Journal of Applied Physics, 96 (2004) 7686-7695

[30] P. Petrik, T. Gumprecht, A. Nutsch, G. Roeder, M. Lemberger, G. Juhasz, O. Polgar, C. Major, P. Kozma, M. Janosov, B. Fodor, E. Agocs and M. Fried, "Comparative measurements on atomic layer deposited Al_2O_3 thin films using ex-situ table top and mapping ellipsometry as well as X-ray and VUV reflectometry", Thin Solid Films, 541 (2013) 131-135

[31] E. Langereis, J. Keijmel, M.C.M. van de Sanden and W.M.M. Kessels, "Surface chemistry of plasma-assisted atomic layer deposition of Al_2O_3 studied by infra-red spectroscopy", Applied Physics Letters, 92 (2008) 231904

[32] K.H. Kwon, A. Efremov, S.J. Sun, I. Chun and K. Kim, "Dry etching characteristics of Mo and Al_2O_3 films in $O_2/Cl_2/Ar$ inductively coupled plasmas", Thin Solid Films, 552 (2014) 105-110

[33] G.G. Stoney, "The tension of metallic films deposited by electrolysis", Proceedings of the Royal Society of London, 9 (1909) 172-175

[34] P. Temple-Boyer, B. Rousset and E. Scheid, "Influences of deposition and crystallization kinetics on the properties of silicon films deposited by chemical vapour deposition from silane and disilane", Thin Solid Films, 518 (2010) 6897-6903

[35] E.D. Palik: "Handbook of optical constant of solids, volume II", Academic press, USA (1998), ISBN: 0-12-544420-6

[36] M. Cho, J. Park, H.-B. Park and C.-S. Hwang, J. Jeong and K.-S. Hyun, "Chemical interaction between atomic-layer-deposited HfO_2 thin films and the Si substrate", Applied Physics Letters, 81 (2002) 334-336

[37] Z.-Y. Wang, R.-J. Zhang, H.-L. Lu, X. Chen, Y. Sun, Y. Zhang, Y.-F. Wei, J.-P. Xu, S.-Y. Wang, Y.-X. Zheng and L.-Y. Chen, "The impact of thickness and thermal annealing on refractive index for aluminium oxide thin films deposited by atomic layer deposition", Nanoscale Research Letters, 10 (2015) 46-51

[38] S. Jakschik, U. Schröder, T. Hecht, M. Gutsche, H. Seidl and J.W. Bartha, "Crystallization behaviour of thin ALD-Al_2O_3 films", Thin Solid Films, 425 (2003) 2016-220

[39] G. Krautheim, T. Hecht, S. Jakschik, U. Schröder and W. Zahn, "Mechanical stress in ALD-Al_2O_3 films", Applied Surface Science, 252 (2005) 200-204

[40] "Metals, Alloys, Compounds, Ceramics, Polymers, Composites, catalogue 1993/1994", Goodfellow Metals Limited, Cambridge, United Kingdom (1993)

Tables and figures captions

Table 1: TEM characterisation of the different structures deposited by PE-ALD from TMA and O_2

Table 2: TEM characterisation of the 600-cycle TMA/O_2 PE-ALD Al_2O_3 films annealed 5 minutes under an O_2 gaseous atmosphere at different temperatures

Table 3: Wet and dry etching properties of Al_2O_3 deposited by PE-ALD from TMA and O_2

Figure 1: Apparent mean growth rate per ALD cycle and refractive index of Al_2O_3 films versus ALD cycle number (parameters were estimated by ellipsometry at a 450nm wavelength)

Figure 2: TEM/EDX investigation of the 60-cycle TMA/O_2 PE-ALD sample evidencing a SiO_2/Al_xSi_yO structure: a) TEM image and b) EDX atomic concentration profiles

Figure 3: TEM/EDX investigation of the 600-cycle TMA/O_2 PE-ALD sample evidencing a Al_xSi_yO/Al_2O_3 structure: a) TEM image and b) EDX atomic concentration profiles

Figure 4: TEM/EDX investigation of the 300-cycle TMA/O_2 PE-ALD sample deposited on an oxidized (SiO_2 thickness: ~10 nm) silicon substrate, evidence of a SiO_2/Al_2O_3 steep structure

Figure 5: TEM/EDX investigation of the 600-cycle TMA/O_2 PE-ALD sample annealed at 750°C under an O_2 atmosphere, evidence of a Si/SiO_2/Al_2O_3 steep structure

Figure 6: Refractive index n_{450nm} of 400-cycle PE-ALD Al_2O_3 films versus annealing temperature

(gaseous atmosphere: N_2/H_2 and O_2)

Figure 7: XRD investigation of the 400-cycle PE-ALD Al_2O_3 sample with annealing temperature:

a) XRD patterns and b) intensity peak height à 67.8°

Figure 8: TEM investigation of the 600-cycle PE-ALD polycrystalline Al_2O_3 sample

annealed 5 minutes under an O_2 gaseous atmosphere at 900°C

Figure 9: Residual stress σ of 900-cycle PE-ALD Al_2O_3 films versus annealing temperature

(gaseous atmosphere: N_2/H_2 and O_2)

Figure 10: Dielectric constant ε_r of 400-cycle PE-ALD Al_2O_3 films versus annealing temperature

(gaseous atmosphere: O_2)

Number of cycles	SiO$_2$ thickness (nm)	Al$_x$Si$_y$O thickness (nm)	Al$_2$O$_3$ thickness (nm)
30	4	2.5	0
60	7	5	0
300	0 *	6	24
600	0 *	6	48
300 (on SiO$_2$)	10	0 *	26

Table 1: TEM characterisation of the different structures deposited by PE-ALD from TMA and O$_2$

(* experimental value lower than the TEM/EDX resolution)

Annealing temperature	SiO_2 thickness (nm)	Al_xSi_yO thickness (nm)	Al_2O_3 thickness (nm)
as-deposited	0 *	6	48
750°C	3	0 *	52
900°C	5	0 *	47

Table 2: TEM characterisation of the 600-cycle TMA/O_2 PE-ALD Al_2O_3 films

annealed 5 minutes under an O_2 gaseous atmosphere at different temperatures

(* experimental value lower than the TEM/EDX resolution)

	etch rate (nm/min)					
	wet etch at ambient temperature		Cl$_2$ dry etch with bias power (ICP power: 500 W)			
	H$_3$PO$_4$ 85%	HF 5%	25 W	50 W	80 W	100 W
amorphous Al$_2$O$_3$	0.4	40	22	40	70	85
polycrystalline Al$_2$O$_3$	~ 0	~ 0	20	38	40	40

Table 3: Wet and dry etching properties of Al$_2$O$_3$ deposited by PE-ALD from TMA and O$_2$
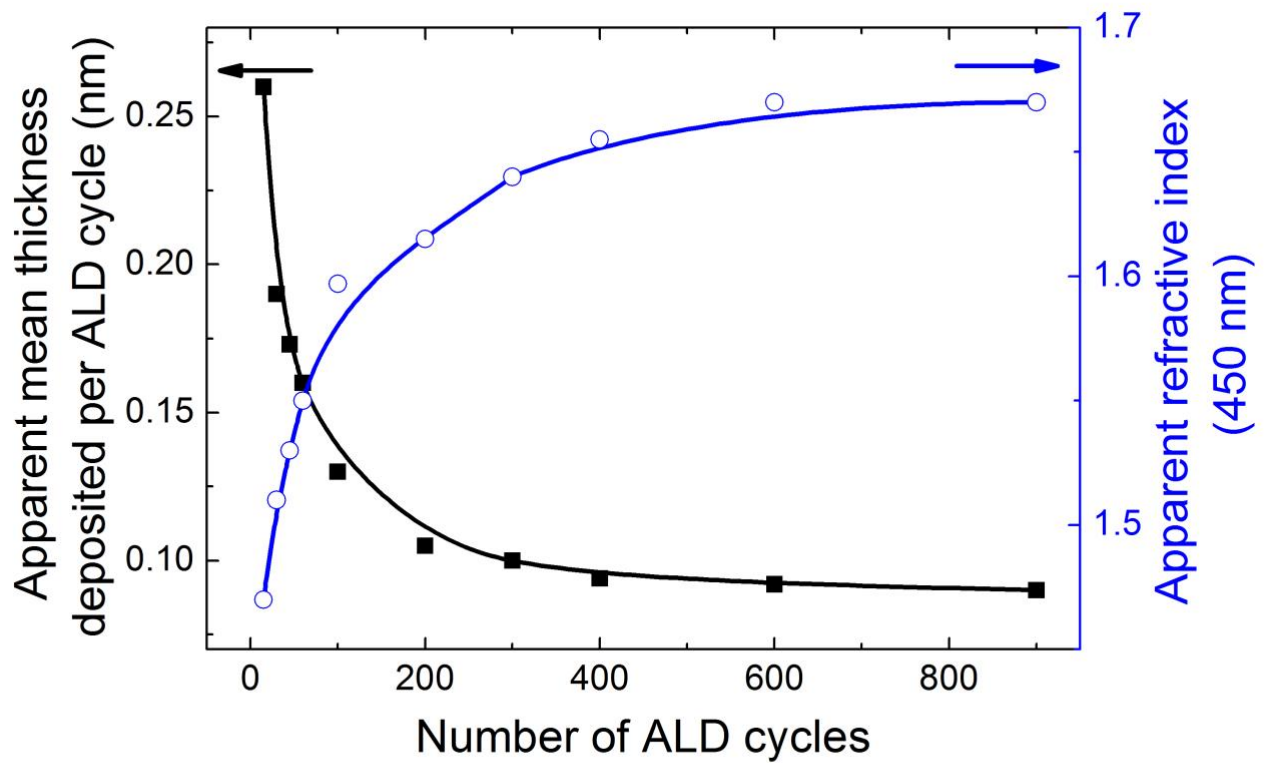
Figure 1: Apparent mean growth rate per ALD cycle and refractive index of Al_2O_3 films versus ALD cycle number (parameters were estimated by ellipsometry at a 450nm wavelength)
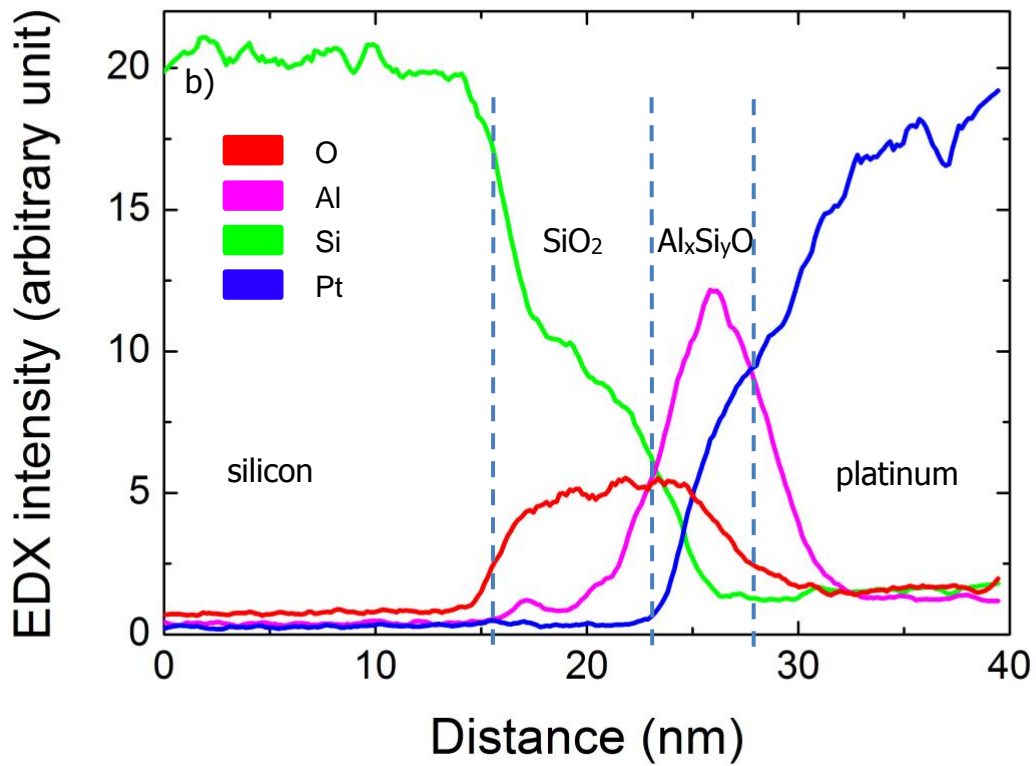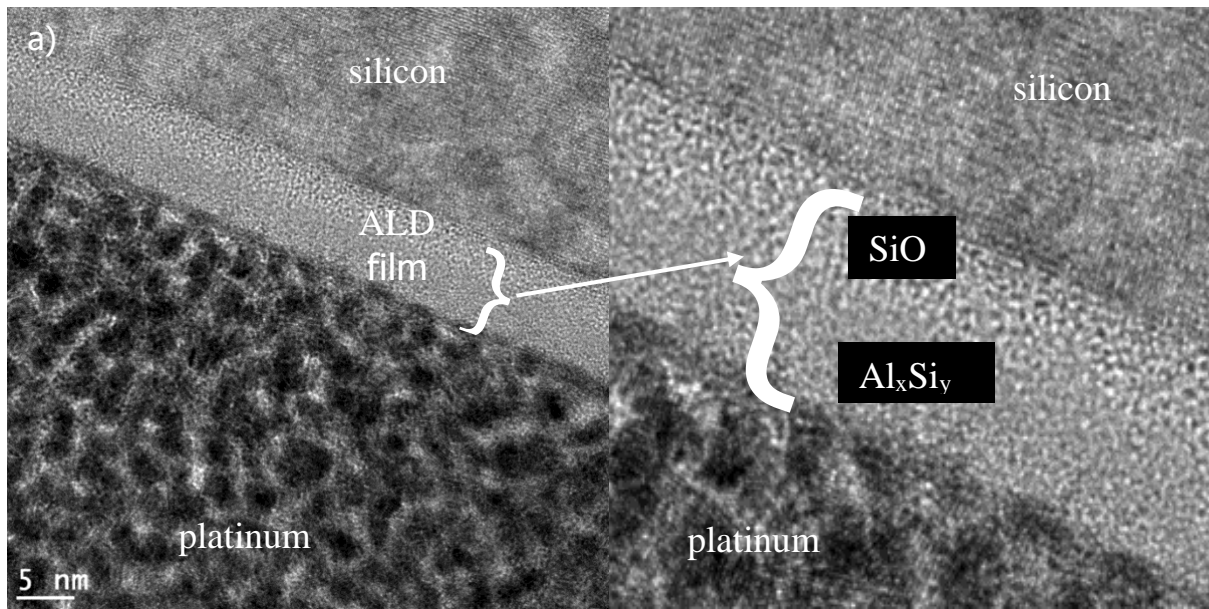
Figure 2: TEM/EDX investigation of the 60-cycle TMA/O_2 PE-ALD sample evidencing an SiO_2/Al_xSi_yO structure: a) TEM image and b) EDX atomic concentration profiles
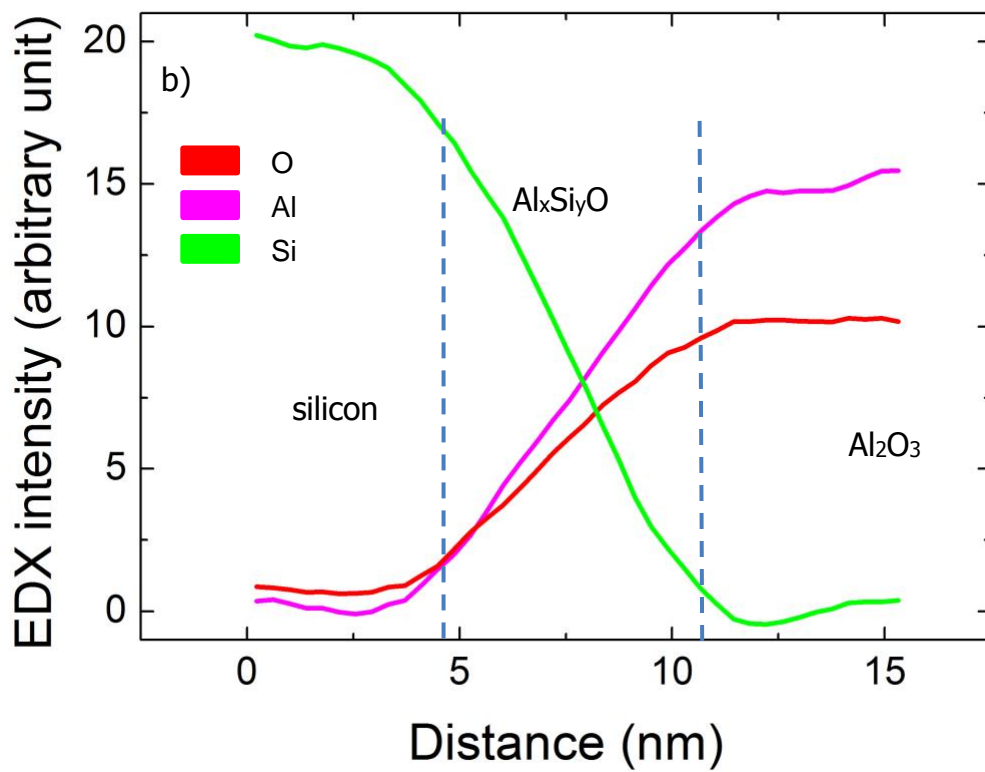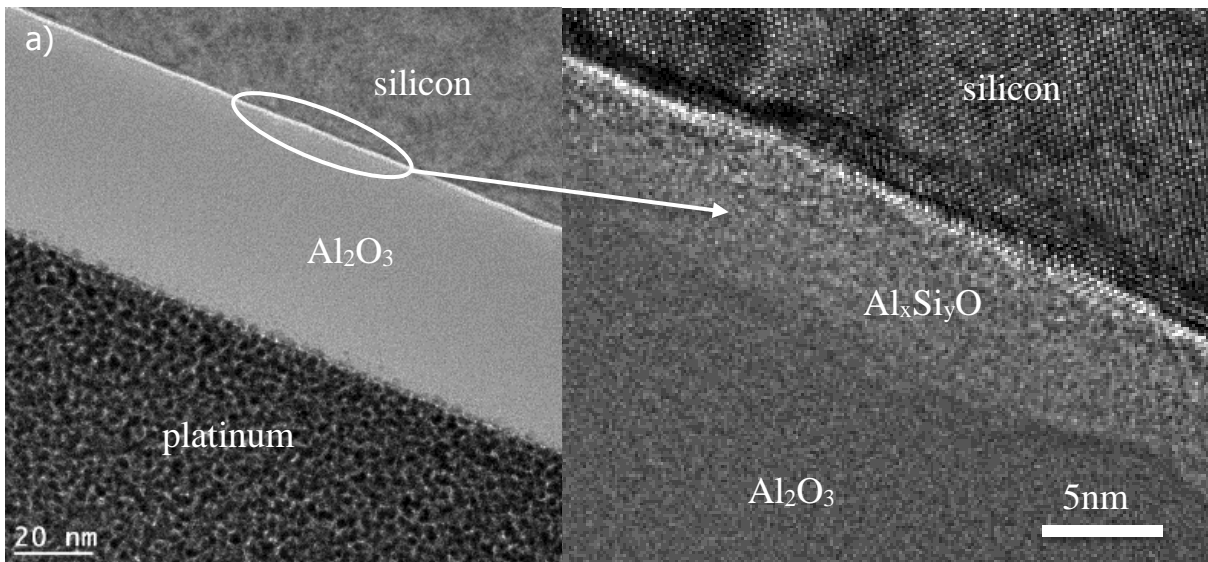
b)

Figure 3: TEM/EDX investigation of the 600-cycle TMA/O_2 PE-ALD sample

evidencing an Al_xSi_yO/Al_2O_3 structure: a) TEM image and b) EDX atomic concentration profiles
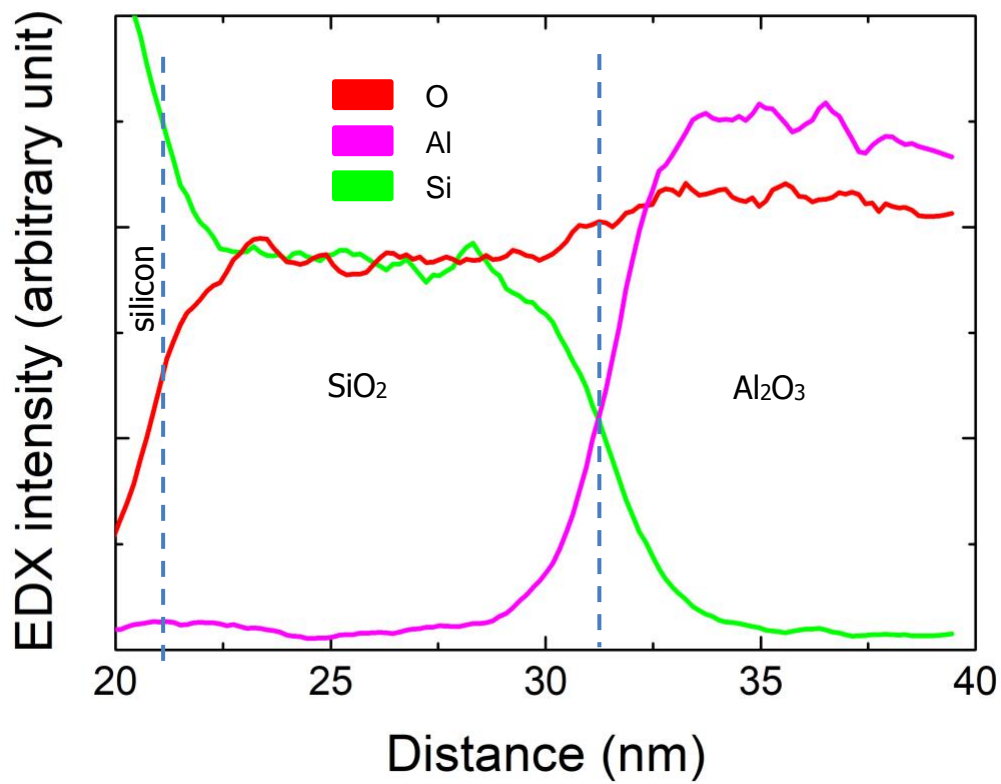
Figure 4: TEM/EDX investigation of the 300-cycle TMA/O_2 PE-ALD sample deposited on an oxidized (SiO$_2$ thickness: ~10 nm) silicon substrate, evidence of a SiO$_2$/Al$_2$O$_3$ steep structure
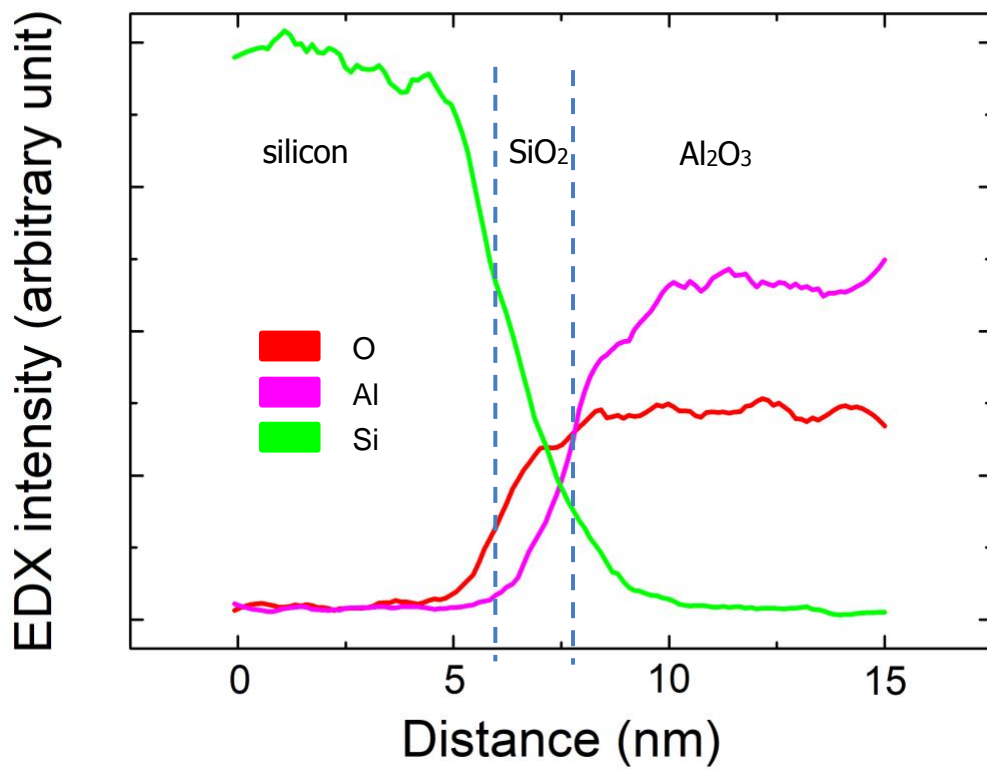
Figure 5: TEM/EDX investigation of the 600-cycle TMA/O_2 PE-ALD sample annealed at 750°C under an O_2 atmosphere, evidence of a Si/SiO_2/Al_2O_3 steep structure

Figure 6: Refractive index n_{450nm} of 400-cycle PE-ALD Al_2O_3 films versus annealing temperature

(gaseous atmosphere: N_2/H_2 and O_2)

a)

b)

c)

Figure 7: XRD investigation of the 400-cycle PE-ALD Al_2O_3 sample with annealing temperature:

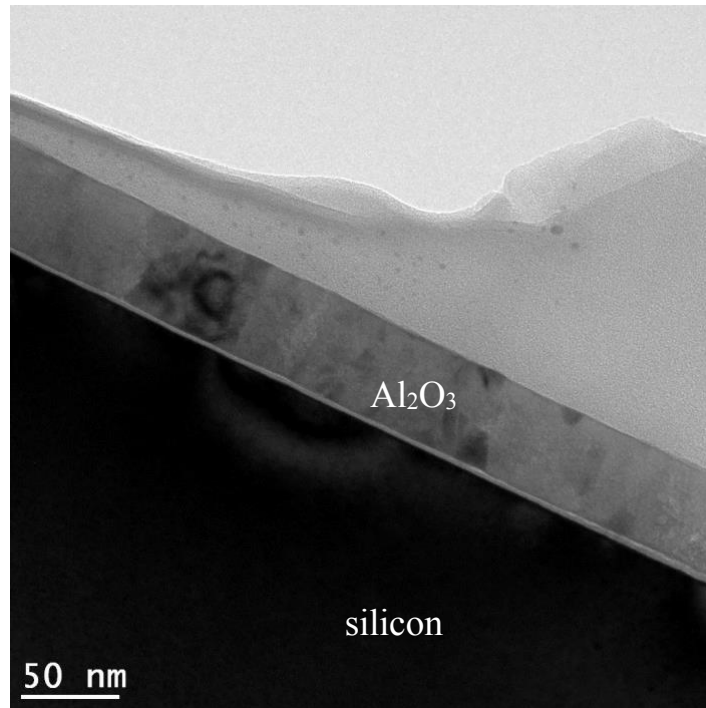a, b) XRD patterns and c) intensity peak height at $67.8°$

Figure 8: TEM investigation of the 600-cycle PE-ALD polycrystalline Al_2O_3 sample annealed 5 minutes under an O_2 gaseous atmosphere at 900°C
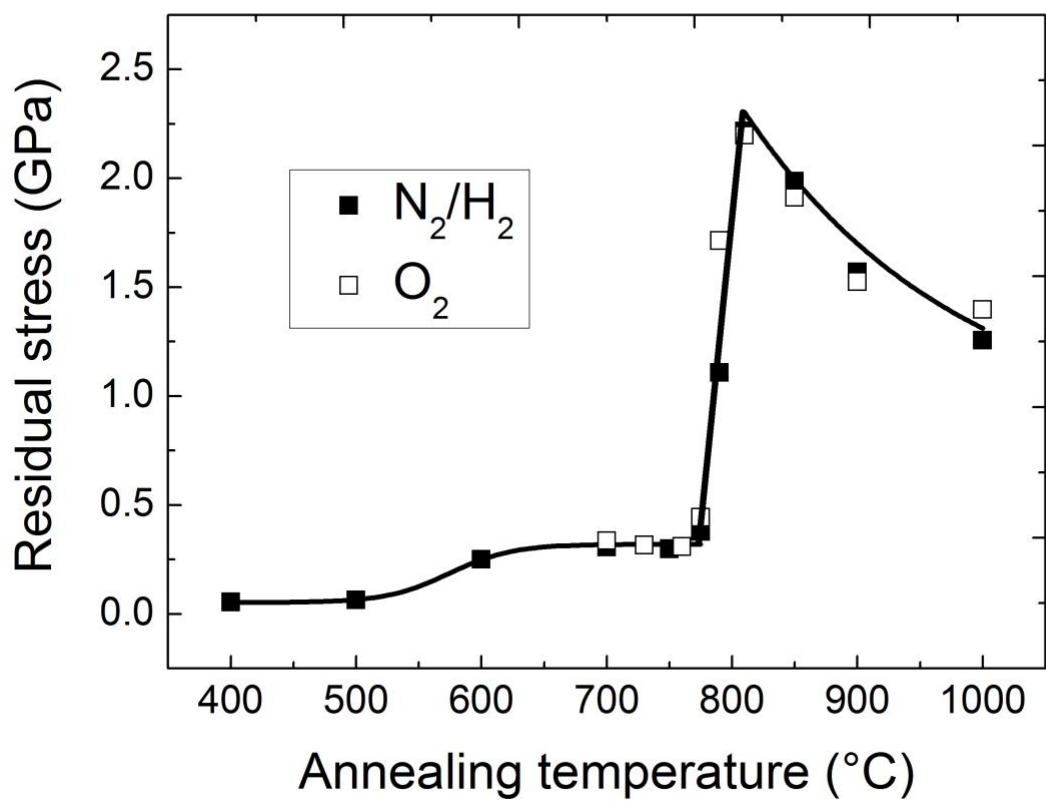
Figure 9: Residual stress σ of 900-cycle PE-ALD Al_2O_3 films versus annealing temperature
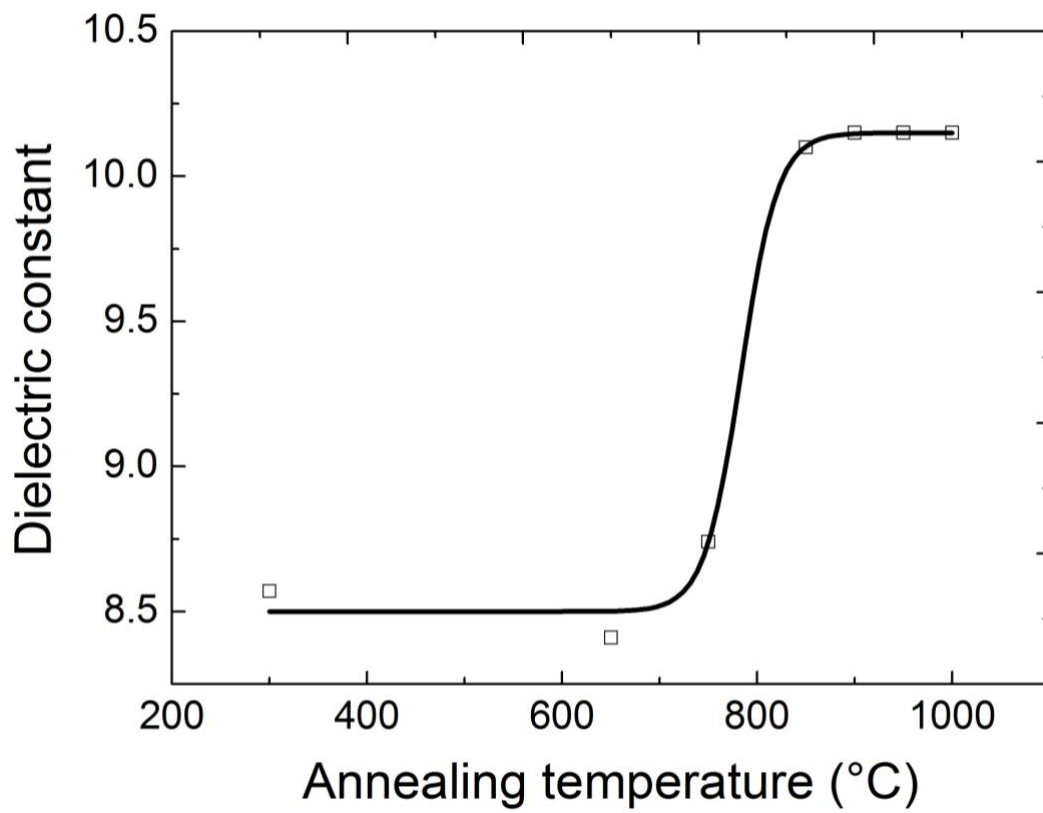
(gaseous atmosphere: N_2/H_2 and O_2)

Figure 10: Dielectric constant ε_r of 400-cycle PE-ALD Al_2O_3 films versus annealing temperature

(gaseous atmosphere: O_2)